J. Fluid Mech. (2005), *vol.* 532, *pp.* 199–216.
doi:10.1017/S0022112005004039 Printed in the United Kingdom

Scalar dissipation rate and dissipative anomaly in isotropic turbulence

By D. A. DONZIS[1,3], K. R. SREENIVASAN[1,2] AND P. K. YEUNG[3]

[1]International Centre for Theoretical Physics, Strada Costiera 11, 34014 Trieste, Italy

[2]Institute for Physical Science and Technology, University of Maryland, College Park, MD 20742, USA

[3]School of Aerospace Engineering, Georgia Institute of Technology, Atlanta, GA 30332, USA

(Received 25 March 2004 and in revised form 4 December 2004)

We examine available data from experiment and recent numerical simulations to explore the supposition that the scalar dissipation rate in turbulence becomes independent of the fluid viscosity when the viscosity is small and of scalar diffusivity when the diffusivity is small. The data are interpreted in the context of semi-empirical spectral theory of Obukhov and Corrsin when the Schmidt number, Sc, is below unity, and of Batchelor's theory when Sc is above unity. Practical limits in terms of the Taylor-microscale Reynolds number, R_λ, as well as Sc, are deduced for scalar dissipation to become sensibly independent of molecular properties. In particular, we show that such an asymptotic state is reached if $R_\lambda Sc^{1/2} \gg 1$ for $Sc < 1$, and if $\ln(Sc)/R_\lambda \ll 1$ for $Sc > 1$.

1. Introduction

After some fifty years of accumulated work (e.g. Batchelor 1953; Sreenivasan 1984, 1995, 1998; Zocchi *et al.* 1994; Kaneda *et al.* 2003), it has now become empirically clear that, away from the walls, the mean dissipation rate of turbulent energy

$$\langle \varepsilon \rangle \equiv \frac{\nu}{2} \left\langle \left(\frac{\partial u_j}{\partial u_i} + \frac{\partial u_i}{\partial u_j} \right)^2 \right\rangle,$$

is independent of the fluid viscosity, ν, as long as ν is small, or the appropriate Reynolds number is large. Here, u_i is the velocity fluctuation in the coordinate direction x_i and $\langle \cdot \rangle$ indicates a suitable average. This property of turbulence (Taylor 1938; Kolmogorov 1941), known as the dissipative anomaly, has the consequence that the normalized energy dissipation, i.e. the function $f \equiv \langle \varepsilon \rangle L / u'^3$, where L and u' are some viscosity-independent length and velocity scales, respectively, approaches an asymptotic constant in the limit of high Reynolds numbers. This behaviour of f is consistent with rigorous bounds for $\langle \varepsilon \rangle$ deduced from the Navier–Stokes equations (e.g. Constantin 1994). In particular, a functional form motivated by the results of Doering & Foias (2002), namely

$$f \equiv \frac{\langle \varepsilon \rangle L}{u'^3} = A(1 + \sqrt{1 + (B/R_\lambda)^2}), \tag{1.1}$$

where $R_\lambda \equiv u' \lambda / \nu$ is the Reynolds number based on the Taylor microscale λ, with $\lambda^2 = u'^2 / \langle (\partial u / \partial x)^2 \rangle$ and $u'^2 \equiv \langle u^2 \rangle$, is found to provide, as seen in figure 1, a good fit for the Reynolds number dependence of f. Here, L is the longitudinal integral length

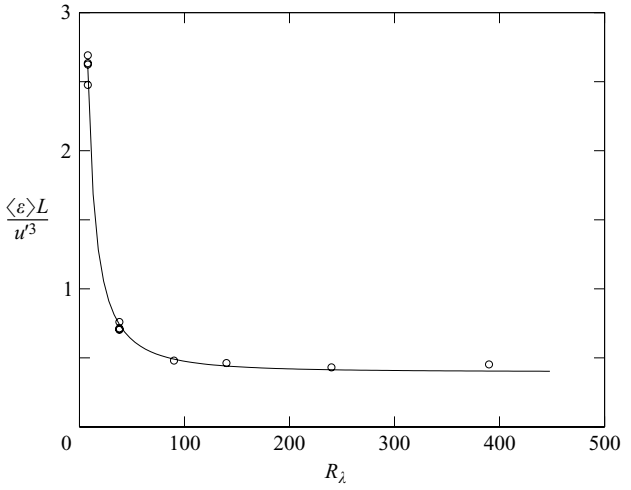

FIGURE 1. Normalized energy dissipation rate from the direct numerical simulations of isotropic turbulence. Solid line represents equation (1.1) with $A \approx 0.2$ and $B \approx 92$.

scale evaluated from the energy spectrum function $E(k)$ in wavenumber space as

$$L = \frac{\pi}{2u'^2} \int_0^\infty \frac{E(k)}{k}\, \mathrm{d}k. \tag{1.2}$$

With this choice, the fit in figure 1 gives $A \approx 0.2$ and $B \approx 92$, yielding an asymptotic value of 0.4 for f.

While the behaviour shown in figure 1 is universal for all turbulent flows away from the solid wall (see Sreenivasan 1995), it must be stressed that the coefficients A and B are not universal, even if one fixes the operational definitions of L and u'. They depend on the type of flow, and, for a given flow, on detailed initial conditions – for example the geometry of the grids in grid-generated turbulence and the nature of large-scale forcing in simulations.

Similar issues can be explored for $\langle\chi\rangle \equiv 2\kappa\langle(\partial\phi/\partial x_i)^2\rangle$, which is the mean 'dissipation' rate of the scalar variance $\langle\phi^2\rangle$, ϕ being the fluctuating scalar and κ its diffusion coefficient. Specifically: (*a*) what is the 'asymptotic' nature of $\langle\chi\rangle$ when ν and κ are both small? (*b*) What is the analogue of (1.1) for $\langle\chi\rangle$ as a function of R_λ and the Schmidt number Sc $(\equiv \nu/\kappa)$? Answering these questions is the goal of this paper. Aside from their intrinsic interest, the findings are of practical value for reacting flows in which the products in the fast-chemistry limit are in direct proportion to χ (see, e.g. Bilger 2004; Sreenivasan 2004).

The questions outlined above are not entirely new, but the available data are scattered in the literature and the effect of Schmidt number, especially for $Sc \gg 1$, has received less attention than is warranted. Monin & Yaglom (1975) discussed (*a*) above, while both (*a*) and (*b*) were addressed briefly by Sreenivasan & Yeung (2000). A short paper addressing some of these same issues (Xu, Antonia & Rajagopalan 2000) has also appeared. We believe, however, that this work is the first comprehensive evaluation of these questions, besides incorporating new data from direct numerical simulations and presenting related correlations. In § 2, we provide a brief overview of numerical and experimental datasets from various sources used in the paper, as well as some basic information on the numerical methods used in the present simulations. In § 3, we present results and theoretical considerations, which lead us to infer the

circumstances under which the scalar dissipation becomes independent of molecular properties, for $Sc < 1$ and $Sc > 1$. Conclusions are summarized in § 4.

2. The data

2.1. *From direct numerical simulations (DNS)*

The velocity field for the present DNS database is homogeneous and isotropic. These data are obtained by solving the Navier–Stokes equations using Fourier pseudo-spectral methods (Rogallo 1981) with periodic boundary conditions in all three directions for solution domains with grid resolution from 64^3 to 1024^3. As described in previous publications (e.g. Yeung & Pope 1989), the forcing is applied to low wavenumbers within a spectral shell of chosen radius k_F. This yields a statistically stationary state with a balance between the energy input due to forcing and dissipation due to molecular viscosity. The particular forcing scheme chosen here was developed by Eswaran & Pope (1988), where more details can be found. Although different forcing schemes have been adopted in the literature (see Yeung & Zhou 1997), their details are known to make no difference to the fundamental scaling of $\langle\varepsilon\rangle$ (Sreenivasan 1998).

For the scalar field, we solve for the fluctuations in the presence of an imposed mean gradient (e.g. Pumir 1994; Overholt & Pope 1996; Brethouwer, Hunt & Nieuwstadt 2003) according to the advection–diffusion equation

$$\frac{\partial\phi}{\partial t} + \boldsymbol{u}\cdot\nabla\phi = -\boldsymbol{u}\cdot\nabla\Phi + \kappa\nabla^2\phi, \tag{2.1}$$

where $\nabla\Phi$ is the mean scalar gradient. A spatially uniform $\nabla\Phi$ allows the scalar fluctuations to remain homogeneous and attain a statistically stationary state. This is made possible because the destruction of scalar variance by the molecular dissipation is balanced against its production through the action of velocity fluctuations on the mean gradient. Because (2.1) is linear, the magnitude of $\nabla\Phi$ has no effect on normalized statistics of the scalar field.

We have accumulated a significant DNS database from simulations previously performed in which the Reynolds and Schmidt numbers were varied independently. Table 1 gives the data from Yeung *et al.* (2002, 2004) and Yeung & Sawford (2002). We have also included new data from a 1024^3 resolution. Overall, we have varied R_λ from about 8 to about 390 while keeping Sc fixed at unity; similarly, we varied Sc from 1/4 to 1024 for R_λ fixed at 8 as well as 38 (Yeung *et al.* 2002, 2004). These parameter combinations are shown in table 1. The adequacy of numerical resolution in DNS is often expressed for the velocity field by the non-dimensional parameter $k_{max}\eta$, where $\eta \equiv (\nu^3/\langle\varepsilon\rangle)^{1/4}$ is the Kolmogorov scale (Kolmogorov 1941) and $k_{max} = \sqrt{2}N/3$ is the highest wavenumber resolved on an N^3 grid. For high-Sc scalar fields, the resolution requirement is expressed by $k_{max}\eta_B$, where $\eta_B \equiv \eta Sc^{-1/2}$ is the Batchelor scale (Batchelor 1959). For a given computational size, this requirement is met only by keeping the Reynolds number appropriately low. For reference, we have included in table 1 the values of u'^2, the scalar variance related to its spectral density E_ϕ through

$$\phi'^2 \equiv \langle\phi^2\rangle = \int_0^\infty E_\phi(k)\,\mathrm{d}k, \tag{2.2}$$

the integral scale for velocity, L, the integral scale for the scalar, L_ϕ, defined through

R_λ	u'	L	$\langle\varepsilon\rangle$	ν	Sc	ϕ'	L_ϕ	$\langle\chi\rangle$	N
8	1.122	1.498	2.537	0.159	1	1.029	1.174	1.410	128
8	1.122	1.498	2.537	0.159	8	1.667	0.847	1.656	128
8	1.122	1.498	2.537	0.159	64	2.208	0.613	1.670	128
8	1.144	1.518	2.588	0.159	4	1.384	0.944	1.449	128
8	1.144	1.518	2.588	0.159	16	1.739	0.765	1.434	128
8	1.144	1.518	2.588	0.159	32	1.897	0.691	1.404	128
8	1.197	1.575	2.697	0.159	64	2.570	0.661	2.177	256
8	1.197	1.575	2.697	0.159	128	2.737	0.601	2.141	256
8	1.197	1.575	2.697	0.159	256	2.895	0.550	2.103	256
8	1.182	1.576	2.760	0.159	256	3.161	0.555	2.494	512
8	1.182	1.576	2.760	0.159	512	3.321	0.511	2.455	512
8	1.182	1.576	2.760	0.159	1024	3.471	0.473	2.416	512
38	1.625	1.077	2.822	0.025	0.25	1.029	0.935	2.106	64
38	1.625	1.077	2.822	0.025	0.5	1.197	0.838	2.285	64
38	1.625	1.077	2.822	0.025	1	1.355	0.751	2.397	64
38	1.589	1.007	2.802	0.025	0.25	1.108	0.994	2.240	256
38	1.589	1.007	2.802	0.025	1	1.433	0.801	2.500	256
38	1.589	1.007	2.802	0.025	4	1.716	0.649	2.568	256
38	1.584	1.064	2.665	0.025	4	1.758	0.628	2.720	256
38	1.584	1.064	2.665	0.025	8	1.893	0.566	2.724	256
38	1.584	1.064	2.665	0.025	16	2.024	0.511	2.723	256
38	1.645	1.214	2.787	0.025	16	2.145	0.530	2.969	512
38	1.645	1.214	2.787	0.025	32	2.271	0.483	2.935	512
38	1.645	1.214	2.787	0.025	64	2.391	0.443	2.903	512
90	1.295	1.366	0.763	0.006546	0.125	1.601	1.102	2.573	128
90	1.295	1.366	0.763	0.006546	0.25	1.750	1.003	2.694	128
90	1.295	1.366	0.763	0.006546	1	2.017	0.829	2.835	128
140	1.404	1.095	1.169	0.0028	0.125	1.263	0.924	1.875	256
140	1.404	1.095	1.169	0.0028	1	1.458	0.731	1.934	256
240	1.480	1.164	1.201	0.0011	0.125	1.807	0.955	3.235	512
240	1.480	1.164	1.201	0.0011	1	1.943	0.827	3.245	512
390	1.534	1.254	1.302	0.000437	0.125	1.641	0.896	2.579	1024
390	1.534	1.254	1.302	0.000437	1	1.714	0.819	2.588	1024

TABLE 1. DNS data in our simulations, from Yeung *et al.* (2002) for $R_\lambda = 8$, Yeung *et al.* (2004) for $R_\lambda = 38$–240, including preliminary results for $R_\lambda = 390$.

the relation

$$L_\phi = \frac{\pi}{2\langle\phi^2\rangle}\int_0^\infty \frac{E_\phi(k)}{k}\,\mathrm{d}k, \tag{2.3}$$

as well as $\langle\varepsilon\rangle$, $\langle\chi\rangle$, R_λ and Sc.

In addition to the present, we incorporate data from Overholt & Pope (1996), Bogucki, Domaradzki & Yeung (1997), Wang, Chen & Brasseur (1999) and Watanabe & Gotoh (2004). All these studies were for stationary isotropic turbulence though some of them differ in the method of forcing the turbulence and in ways by which scalar fluctuations are maintained against scalar dissipation. Bogucki *et al.* (1997) forced both the velocity and scalar field by keeping the energy constant in a few low-wavenumber modes. The forcing of the velocity field by Overholt & Pope was the same as the present, as was the manner of maintaining stationarity of the scalar field through the mean gradient. Wang *et al.* maintained both the velocity and scalar fields stationary by forcing wavenumbers with $k < 3$ such that the energy and scalar spectra followed a $k^{-5/3}$ power law. Watanabe & Gotoh forced both the velocity and scalar

R_λ	u'	L	$\langle\varepsilon\rangle$	ν	Sc	ϕ'	L_ϕ	$\langle\chi\rangle$	N
258	1.077	1.180	0.507	0.0006	1	1.421	0.407	1.116	512
427	1.146	1.180	0.591	0.00024	1	1.407	0.413	1.196	1024

TABLE 2. DNS data from Watanabe & Gotoh (2004).

R_λ	u'	L	$\langle\varepsilon\rangle$	ν	Sc	ϕ'	L_ϕ	$\langle\chi\rangle$	N
28	0.902	1.260	0.519	0.025	0.7	1.424	1.424	1.539	32
52	2.497	1.091	8.703	0.025	0.7	1.476	1.477	4.136	64
84	6.266	0.965	132.300	0.025	0.7	1.421	1.421	9.856	128
84	6.187	0.970	126.500	0.025	0.7	1.375	1.375	9.012	128

TABLE 3. DNS data from Overholt & Pope (1996). The integral scalar length in their paper is taken to be $L_\phi = \langle\phi^2\rangle^{1/2}/\beta$, which is reproduced here.

R_λ	u'	L	$\langle\varepsilon\rangle$	ν	Sc	ϕ'	L_ϕ	$\langle\chi\rangle$	N
132	0.676	1.072	0.179	0.001	0.7	0.766	0.752	0.345	256
68	0.256	1.049	0.014	0.001	0.7	0.141	0.883	0.004	256
100	0.857	1.530	0.201	0.004	1	1.090	0.956	0.419	128
151	0.855	1.514	0.177	0.002	1	1.090	0.937	0.440	256
195	0.874	1.412	0.246	0.001	1	1.100	0.918	0.501	512

TABLE 4. DNS data from Wang *et al.* (1999).

R_λ	u'	L	$\langle\varepsilon\rangle$	ν	Sc	ϕ'	L_ϕ	$\langle\chi\rangle$	N
36	0.450	1.310	0.047	0.01	3	0.905	0.711	0.160	162
36	0.450	1.310	0.047	0.01	5	0.984	0.506	0.190	162
36	0.450	1.310	0.047	0.01	7	1.001	0.648	0.160	162
74	0.560	1.090	0.080	0.0033	3	1.010	0.715	0.260	240
74	0.560	1.090	0.080	0.0033	5	1.060	0.650	0.260	240
74	0.560	1.090	0.080	0.0033	7	1.080	0.642	0.270	240

TABLE 5. DNS data from Bogucki *et al.* (1997).

field with Gaussian random solenoidal forces that were delta-correlated in time, and applied the forcing in the wavenumber range $1 \leqslant k \leqslant 2$. The relevant parameters from these references are summarized in tables 2 to 5, making sure (except when explicitly noted otherwise) that they conform to the definitions used here.

2.2. *From experiment*

The data considered here are from Mills *et al.* (1958), Yeh & Van Atta (1973), Warhaft & Lumley (1978), Sreenivasan *et al.* (1980), Tavoularis & Corrsin (1981), Sirivat & Warhaft (1983), Mydlarski & Warhaft (1998) and Antonia, Zhou & Xu (2000) (table 6). Most of the measurements were made at low Reynolds numbers and for nearly passive temperature fluctuations in air ($Sc \approx 0.7$) in decaying grid-turbulence, generated by heating either the turbulence-generating grid itself, or an auxiliary screen placed downstream; the experimental configurations and conditions are succinctly summarized by Sreenivasan *et al.* (1980). The recent experiments of Mydlarski & Warhaft (1998) stretch the Reynolds number range substantially using the so-called

Source	R_λ	u'	L	$\langle\varepsilon\rangle$	ν	Sc	ϕ'	L_ϕ	$\langle\chi\rangle$
MKOC	22	0.0529	0.0157	0.016	1.5	0.72	0.075	0.0142	0.0199
YV	35	0.0872	0.02	0.0456	1.55	0.725	0.2776	0.0184	0.308
WL	45	0.121	–	0.0951	1.65	0.73	0.0687	–	0.01298
	45	0.121	–	0.0951	1.65	0.73	0.1105	–	0.0558
STHC	34	0.1	0.014	0.0856	1.5	0.71	0.0549	0.0116	0.0203
	34	0.1	0.014	0.0856	1.5	0.71	0.135	0.0111	0.132
TC	128	0.4227	0.044	1.94	1.5	0.71	0.1091	0.031	0.128
	147	0.4889	0.051	2.65	1.5	0.71	0.1158	0.038	0.154
	160	0.5441	0.057	3.42	1.5	0.71	0.1249	0.0435	0.1773
SW	26	0.0432	0.02	0.00531	1.65	0.7	0.02963	0.0156	0.00222
	36	0.08	0.02	0.0393	1.65	0.7	0.0576	0.0164	0.0176
MW	85	0.1249	0.056	0.0314	1.6	0.71	0.249	0.052	0.124
	140	0.1703	0.11	0.0418	1.55	0.69	0.4195	0.17	0.277
	247	0.3162	0.17	0.164	1.5	0.67	0.5797	0.16	0.581
	306	0.3018	0.3	0.0833	1.6	0.71	0.8944	0.33	0.799
	407	1.0198	0.16	6.13	1.6	0.71	0.2828	0.079	0.466
	582	0.7635	0.43	0.94	1.6	0.71	1.0344	0.29	1.74
	731	1.2	0.4	3.88	1.5	0.67	1.4318	0.28	4.96
AZX	30	0.0594	0.0212	0.018	1.5	0.7	0.061	0	0.01
	51	0.1125	0.0465	0.117	1.5	0.7	0.076	0	0.03
	62	0.1809	0.0372	0.4	1.5	0.7	0.061	0	0.032
	78	0.2657	0.0349	1.412	1.5	0.7	0.044	0	0.026

TABLE 6. Experimental data. The scalar integral length scale in Mydlarski & Warhaft (1998) is $L_\phi = \langle\phi^2\rangle^{1/2}/\beta$ where β is the mean gradient.

active grid. The definitions of length and velocity scales used in experiments are sometimes different from those of numerical simulations, which complicates precise comparisons, though these differences do not appear to be critical. In any case, we have provided a list of the different definitions used by the authors wherever necessary or appropriate.

3. The scaling of scalar dissipation

3.1. *Unity Schmidt number*

In analogy to the energy dissipation rate, we can examine the R_λ-variation of $\langle\chi\rangle L/\langle\phi^2\rangle u'$. No general results are known on bounds on scalar dissipation, comparable to those of Doering & Foias (2002) for the energy dissipation, though Schumacher, Sreenivasan & Yeung (2003) studied related issues with the assumption of rapid straining at small scales. The data culled from table 1 for $Sc = 1$, plotted in figure 2, indeed have the form

$$\frac{\langle\chi\rangle L}{\langle\phi^2\rangle u'} = A'(1 + \sqrt{1 + (B'/R_\lambda)^2}), \tag{3.1}$$

which is a direct extension of (1.1). For our own DNS data (circles in the figure) we have $A' \approx 0.4$ and $B' \approx 31$. The value of B' in (3.1) is significantly smaller than B in (1.1), which suggests that the asymptotic value of the normalized scalar dissipation is attained faster in R_λ than the normalized energy dissipation. This is evident also from a comparison of figures 1 and 2. In analogy with the energy dissipation, we

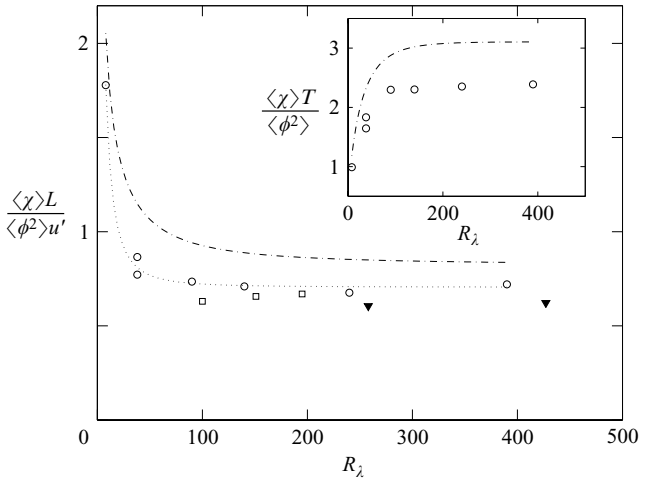

FIGURE 2. Scalar dissipation rate normalized with L/u' for $Sc = 1$. ○, present data; ▼, Wang *et al.* (1999); □, Watanabe & Gotoh (2004). Dotted line: equation (3.1) as the best fit for the present data. Dash-dotted line: theoretical prediction of (3.12), which will be described towards the end of § 3.2. Inset shows the present data using the normalization of T instead of L/u', as well as (3.12). While the asymptotic constancy holds for both normalizations, the direction of approach of this constancy is different.

expect the form of the equation to be the same for all initial conditions, though the numerical values could be different.

In plotting figure 2, we have used L as the relevant lengthscale because the ratio L_ϕ/L is of the order unity for these data (0.7 ± 0.06). Further, instead of using L/u' as the indicator of the large-eddy time scale, we can consider the alternative quantity given by $T \equiv K/\langle\varepsilon\rangle$. Its reciprocal is called the 'mechanical-to-scalar time scale ratio', often used in the modelling of reacting flows (see, e.g. Fox 2003), and has been studied, for example, in Yeung & Sawford (2002). The time scales L/u' and T are related from definitions as

$$\frac{L}{Tu'} = \tfrac{2}{3} f, \tag{3.2}$$

where f is given by (1.1). Because their ratio becomes a constant only for large R_λ, the use of the time scale T, instead of L/u', changes the form of the normalized data for low R_λ, but its constancy for high Reynolds numbers is assured, as seen from the inset to figure 2. The use of T as a time scale possesses an advantage, as we shall see further below.

In summary, it appears from the data just considered that dissipative anomaly applies to passive scalar fields as well. Following the idealized notion of cascades, the implication is also that the time taken by the scalar variance to reach the dissipative scales is of the same order as the time scale of the large eddies. In particular, the present evidence does not support the idea of a cascade short-circuit (Villermaux, Innocenti & Duplat 2001), though it is possible that the present homogeneous flows and the jet flow studied by Villermaux *et al.* could be different in this respect. We have focused here on homogeneous flows partly because the large body of data available allows definitive conclusions to be drawn, and partly because – based on our experience with the energy dissipation (Sreenivasan 1995) – each inhomogeneous flow has to be studied carefully on its own merit. While we do not expect a large qualitative difference, this is clearly work for the future.

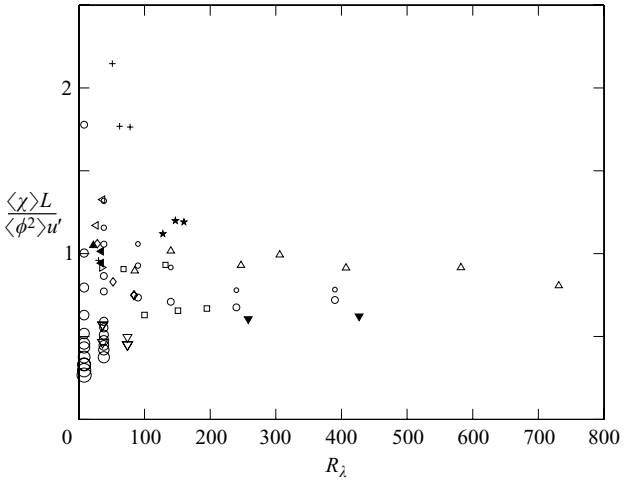

FIGURE 3. Scalar dissipation rate normalized with L/u'. ○, present data; ▼, Watanabe & Gotoh (2004); □, Wang *et al.* (1999); ◇, Overholt & Pope (1996); △, Mydlarski & Warhaft (1998); ★, Tavoularis & Corrsin (1981); ◁, Sirivat & Warhaft (1983); ◀, Sreenivasan *et al.* (1980); ▷, Yeh & Van Atta (1973); ▶, Warhaft & Lumley (1978); ▲, Mills *et al.* (1958); +, Antonia *et al.* (2000); ▽, Bogucki *et al.* (1997). The relative sizes of symbols of the same type illustrate the relative magnitudes of *Sc*.

3.2. *Non-unity Schmidt numbers*

We can now plot available data for all *Sc* in a similar manner (figure 3). The data for different conditions tend to approach constant values of the order unity for large R_λ, though without collapsing, because of the additional parameter, *Sc*. There is, in particular, no discernible order for low R_λ. Instead of examining the R_λ-variation, we may plot the data against the microscale Péclet number

$$P_{\lambda\phi} \equiv \frac{u'\lambda_\phi}{D} = R_\lambda Sc\frac{\lambda_\phi}{\lambda}, \tag{3.3}$$

where the scalar microscale λ_ϕ is defined through the relation

$$\lambda_\phi^2 = 6\kappa\frac{\langle\phi^2\rangle}{\langle\chi\rangle}. \tag{3.4}$$

That, too, does not collapse the data although the dependence on *Sc* emerges more clearly (figure 4). This is not surprising because the Péclet number does not distinguish between the case of low *Sc* and high R_λ on the one hand and that of high *Sc* and low R_λ on the other – which are two different problems in mixing. Even if T were used instead of L/u', the data do not collapse against R_λ or $P_{\lambda\phi}$ (see figures 5 and 6). While a reasonable conclusion may still be that an asymptotic state is reached for large R_λ or $P_{\lambda\phi}$, this limit is not the same for all the data.

For the data used in figure 2, the ratio L_ϕ/L is about 0.7 ± 0.06, so it is reasonable to assume that the scalar field is forced at essentially the same scale as the velocity field. As shown in figure 7, the length scale ratio for our data depends on *Sc*, even if not very strongly.† If L_ϕ/L is small compared to unity so that the scalar forcing

† This dependence may seem surprising at first, but the increasing importance with *Sc* of the -1 part of $E_\phi(k)$ makes it quite plausible. There is practically no dependence on R_λ for fixed *Sc*.

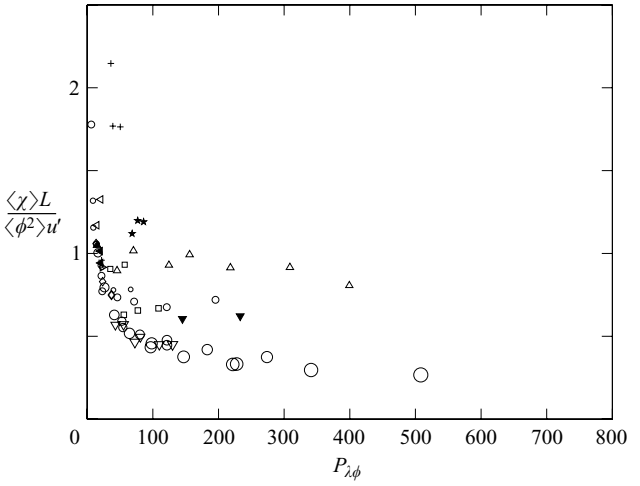

FIGURE 4. Scalar dissipation rate normalized with L/u'. Symbols as in figure 3.

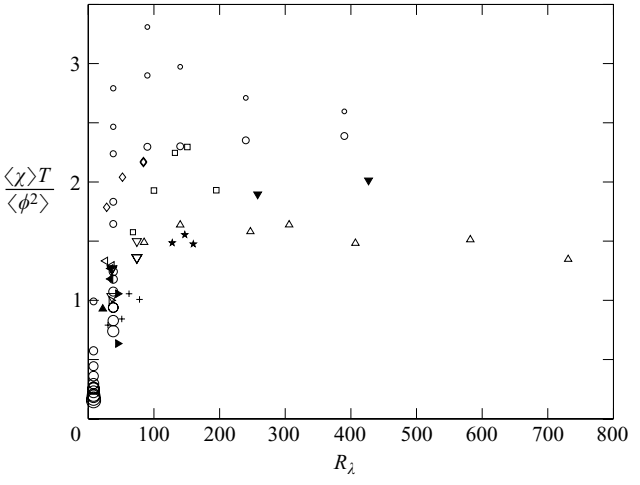

FIGURE 5. Scalar dissipation rate normalized with $T = K/\langle\varepsilon\rangle$. Symbols as in figure 3.

occurs within the inertial range of the velocity field, the appropriate time scale for normalizing $\langle\chi\rangle/\langle\phi^2\rangle$ is not L/u' or T, but their products with the factor $(L_\phi/L)^{2/3}$. This conclusion follows if we assume that the characteristic time scale for the inertial range is given by the Kolmogorov scenario, and that the time scale needed for scalar variance to reach the dissipative scales is diminished because the forcing occurs in the inertial range at $L_\phi < L$. It would thus seem appropriate to multiply the ordinates in figures 3 to 6 by $(L_\phi/L)^{2/3}$. We have prepared these plots, but do not present them because they make no qualitative difference. We surmise the reason to be that, while the length scale ratio is not strictly unity, its variation is not sufficiently strong for it to matter in the present context.

To understand the Sc-dependence of $\langle\phi^2\rangle/\langle\chi\rangle T$, we consider large Sc and small Sc separately. For the former case, we may approximate the scalar spectrum by

$$E_\phi(k) = C_{OC}\langle\chi\rangle\langle\varepsilon\rangle^{-1/3}k^{-5/3} \tag{3.5}$$

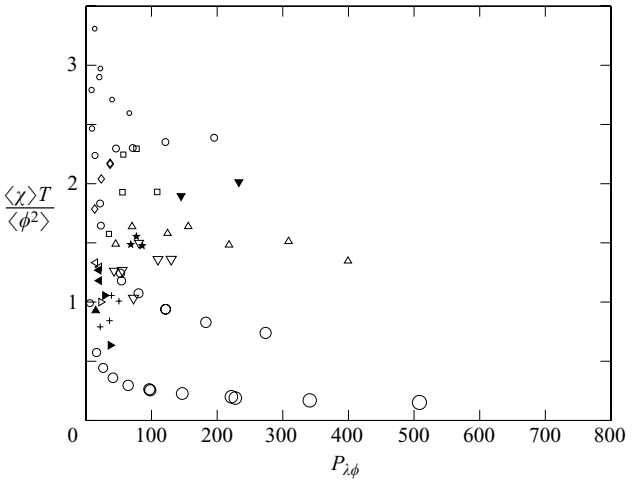

FIGURE 6. Scalar dissipation rate normalized with $T = K/\langle\varepsilon\rangle$. Symbols as in figure 3.

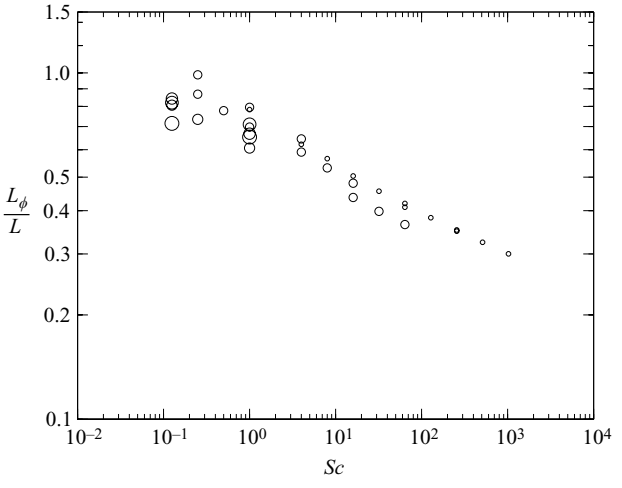

FIGURE 7. Ratio of integral length scales for present data. The relative size of the symbol illustrates the relative magnitude of R_λ.

below a crossover wavenumber and by

$$E_\phi(k) = C_B\langle\chi\rangle(\nu/\langle\varepsilon\rangle)^{1/2}k^{-1} \tag{3.6}$$

above the crossover. Here, C_{OC} is the Obukhov–Corrsin constant (Obukhov 1949; Corrsin 1951) and C_B is the Batchelor constant (Batchelor 1959). The natural crossover scale is $k_\eta \sim 1/\eta$, where $\eta = (\nu^3/\langle\varepsilon\rangle)^{1/4}$ is the Kolmogorov scale. By integrating the scalar spectrum it is then easy to show that

$$\frac{\langle\phi^2\rangle}{\langle\chi\rangle} = \frac{(3/2)C_{OC}}{\langle\varepsilon\rangle^{1/3}k_0^{2/3}}\left[1 - \left(\frac{k_0}{k_\eta}\right)^{2/3}\right] + (1/2)C_B\left(\frac{\nu}{\langle\varepsilon\rangle}\right)^{1/2}\ln(Sc), \tag{3.7}$$

which can be written as

$$\frac{\langle\phi^2\rangle}{\langle\chi\rangle T} = c_1\tilde{f} + c_2\,\frac{\ln(Sc)}{R_\lambda} \tag{3.8}$$

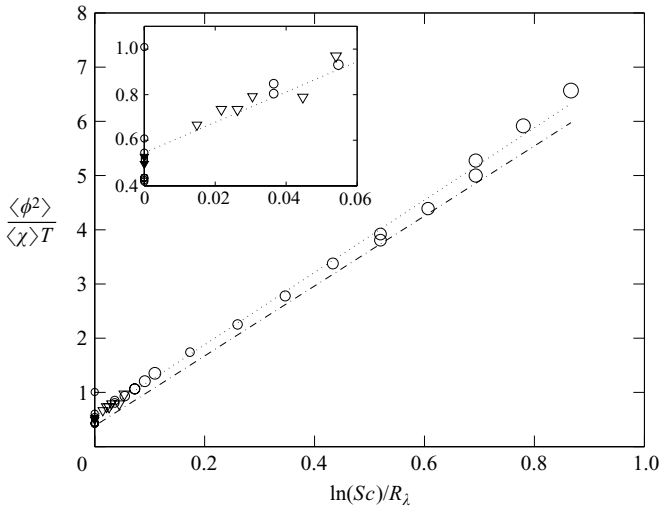

FIGURE 8. High Schmidt number scaling for low and moderate Reynolds numbers. Symbols as in figure 3. Dotted line: best fit for data with $Sc \geqslant 1$. Dash-dotted: equation (3.8) with $C_{OC} = 0.6$ and $C_B = 5$. Inset is an expanded view near the origin. As in figure 3, the relative size of the symbol illustrates the relative magnitude of Sc.

with

$$\tilde{f} = f^{2/3} - \frac{c_3}{R_\lambda}, \tag{3.9}$$

where f comes from (1.1), $c_1 = C_{OC}$, $c_2 = C_B\sqrt{15}/3$ and $c_3 = \sqrt{15}$. It should be noted that taking the crossover scale as a multiple of k_η different from unity – as is indeed suggested by the numerical constants C_{OC} and C_B (determined, e.g. from the simulations of Yeung *et al.* 2002) – does not alter any of the conclusions drawn here. The appearance of terms of the form $1/R_\lambda$ and $\ln(Sc)/R_\lambda$ in (3.9) and (3.10) is also in agreement with a separate analysis by Borgas *et al.* (2004; see equation (15) therein).

The first term of (3.8) depends on both R_λ and the flow (through constants A and B that are implicit in f), and the second term is a linear function of $\ln(Sc)/R_\lambda$. The advantage of using T instead of L/u' is that the prefactor for the second term is a constant in the former case instead of being a function of R_λ and of A and B in the latter. Equation (3.8) shows that the meaning of large Reynolds number for large Sc is that $\ln(Sc)/R_\lambda$ must be small (in addition to the usual criterion that R_λ itself be large).

In simulations given in table 1, it is generally the case that $\ln(Sc)/R_\lambda$ is not small (as we shall discuss further in § 3.3), and so the asymptotic state has not been reached. Nevertheless, for some sets of data, the $\tilde{f}$-term is small compared with the $\ln(Sc)/R_\lambda$-term, which suggests that the data for those cases may collapse if plotted against $\ln(Sc)/R_\lambda$. This is indeed the case, as shown in figure 8.

For $Sc < 1$, we can obtain an approximate spectrum from (3.5), but using the high-wavenumber cut-off at the Obukhov–Corrsin scale ($\eta_{OC} \equiv \eta Sc^{-3/4}$). Proceeding as before, we integrate the spectrum using (1.1) for $\langle\varepsilon\rangle$ and obtain

$$\frac{\langle\phi^2\rangle}{\langle\chi\rangle T} = c_1\left(f^{2/3} - \sqrt{15}\frac{1}{R_\lambda Sc^{1/2}}\right). \tag{3.10}$$

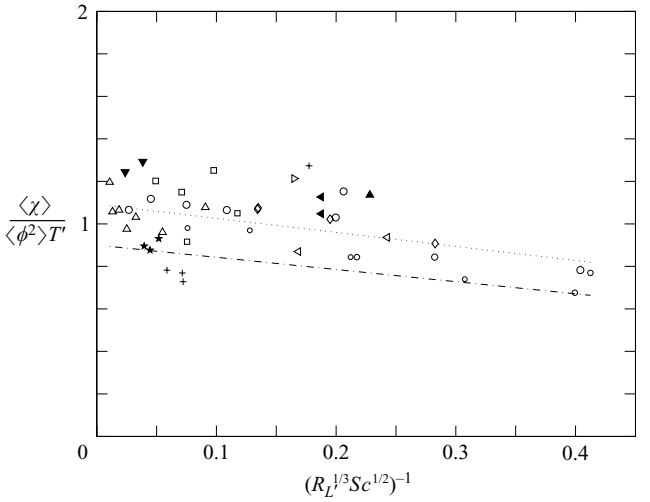

FIGURE 9. Low Schmidt number scaling. Symbols as in figure 3. Dotted line: best fit for data with $Sc < 1$. Dash-dotted: equation (3.11) with $C_{OC} = 0.6$ and $C_B = 5$.

The first term is a function of both the flow geometry (or forcing scheme in simulations) and R_λ, while the second is a linear function of the parameter $(R_\lambda Sc^{1/2})^{-1}$. However, since the first term is in general not small, especially for high R_λ, the straight lines would depend on flow features and R_λ. It is clear that the asymptotic state is attained only when $R_\lambda Sc^{1/2}$ is large (in addition to R_λ being large) – this being different from the large-Sc case.

As an aside, it is worth remarking that (3.10) can be rewritten, using (1.1) for f, as

$$\frac{\langle\phi^2\rangle}{\langle\chi\rangle T'} = \tfrac{3}{2}c_1\left(1 - 15^{-1/6}\frac{1}{R_{L'}^{1/3}Sc^{1/2}}\right), \tag{3.11}$$

where a new time scale $T' = L^{2/3}/\langle\varepsilon\rangle^{1/3}$ and a new Reynolds number $R_{L'} = (u'L^2/\lambda)/\nu$ have been introduced. To obtain this equation, we have also used the relation $R_\lambda f^{2/3} = 15^{2/3}R_{L'}^{1/3}$. The important feature of (3.11) is that it does not contain any flow-dependent parameters (unlike (3.10) through f). If we now plot $\langle\phi^2\rangle/\langle\chi\rangle T'$ against $(R_{L'}^{1/3}Sc^{1/2})^{-1}$ we expect a straight line with a negative slope. In figure 9, we show all the relevant data and compare the best fit (dotted line) with the line given by (3.11) (dash-dotted line with $C_{OC} = 0.6$ and $C_B = 5$). The comparison is not unreasonable. This scaling is a consequence of the Obukhov–Corrsin spectrum, according to which the scalar dissipation rate, when normalized by T', should scale with $R_{L'}^{-1/3}Sc^{-1/2}$, thus independent of all other details. If we plot the data using R_λ, or another time scale, then the dependencies on the flow and R_λ will reappear.

Finally, for $Sc = 1$, we can put Sc to unity in both estimates (3.8) and (3.10), the corresponding form turns out to be the same:

$$\frac{\langle\chi\rangle T'}{\langle\phi^2\rangle} = \frac{2}{3c_1}\left(1 - \frac{15^{-1/6}}{R_{L'}{}^{1/3}}\right)^{-1}. \tag{3.12}$$

We can express (3.12) in terms of L/u' and R_λ as $\langle\chi\rangle L/\langle\phi^2\rangle u' = 2f/(3\ c_1(f^{2/3} - \sqrt{15}/R_\lambda)^{-1})$. This functional form, although different from (3.1), can also be fitted to

compare with the DNS data. In figure 2, we included this theoretical prediction using the values of A and B obtained from our DNS data. This trend of the curve is similar to (3.1), though it yields a somewhat higher value than that observed for the data.

3.3. *Limits*

The results of the preceding section can be summarized as follows:

$$\frac{\langle\phi^2\rangle}{\langle\chi\rangle T}\frac{1}{c_1} = f^{2/3} - \frac{1}{R_\lambda} \times \begin{cases} c_3 - c_4 \ln(Sc) & (Sc > 1), \\ \sqrt{15}\, Sc^{-1/2} & (Sc < 1), \end{cases} \tag{3.13}$$

where $c_4 = c_2/c_1$. We are now interested in the limiting behaviours of $\langle\phi^2\rangle/\langle\chi\rangle T'$ with respect to R_λ and Sc. In particular, from (3.13) it is easy to find the following results:

$$\lim_{R_\lambda\to\infty} \frac{\langle\phi^2\rangle}{\langle\chi\rangle T} = c_1(2A)^{2/3} \quad (0 < Sc < \infty), \tag{3.14}$$

$$\lim_{R_\lambda\to 0} \frac{\langle\phi^2\rangle}{\langle\chi\rangle T} = -c_1\frac{1}{R_\lambda} \begin{cases} c_3 - c_4 \ln(Sc) & (Sc > 1), \\ \sqrt{15}\, Sc^{-1/2} & (Sc < 1), \end{cases} \tag{3.15}$$

$$\lim_{Sc\to\infty} \frac{\langle\phi^2\rangle}{\langle\chi\rangle T} = \frac{1}{R_\lambda} c_2 \ln(Sc) \quad (R_\lambda < \infty), \tag{3.16}$$

$$\lim_{Sc\to 0} \frac{\langle\phi^2\rangle}{\langle\chi\rangle T} = -\frac{c_1\sqrt{15}}{R_\lambda Sc^{1/2}} \quad (R_\lambda < \infty). \tag{3.17}$$

Some comments on these limits are now in order. According to (3.14), as R_λ approaches infinity, the normalized scalar dissipation rate tends to a constant. As already remarked, this constant is flow-dependent. However, the limiting behaviour appears to be independent of the diffusivity of the scalar. In figure 5, this is what would be expected for higher R_λ. In the opposite limit of vanishing R_λ, equation (3.15) shows that the behaviour at small R_λ depends upon Sc (and this dependence is different for scalars with Sc greater or less than unity). Moreover, $\langle\phi^2\rangle/\langle\chi\rangle T$ decreases for $Sc < 1$, while it increases for high Sc (the numerical value depending on c_1 and c_2). This can also be seen in For low-Sc scalars the normalized scalar dissipation increases as R_λ decreases, while high-Sc scalars do the opposite. This limit presents no dependence on the flow (or forcing in DNS). The third limit, (3.16), implies that no flow and forcing effects are felt when Sc is very high. This feature cannot be tested here since the only high-Sc data available are our own, for which a common forcing scheme was used. Finally, (3.17) suggests an R_λ-dependence, but no flow-dependence, as $Sc \to 0$.

We have seen that, according to the Obukhov–Corrsin scaling, there is a universal behaviour of $\langle\chi\rangle/\langle\phi^2\rangle$ when normalized by T' and plotted against $R_{L'}$. This is seen in the recast form of (3.13) as

$$\frac{\langle\phi^2\rangle}{\langle\chi\rangle T'}\frac{2}{3c_1} = 1 - \frac{15^{-2/3}}{{R_{L'}}^{1/3}} \times \begin{cases} c_3 - c_4 \ln(Sc) & (Sc > 1), \\ \sqrt{15}\, Sc^{-1/2} & (Sc < 1). \end{cases} \tag{3.18}$$

Using this form of normalization and remembering that, because of the relation $R_\lambda f^{2/3} = 15^{2/3} {R_{L'}}^{1/3}$, one Reynolds number tends to infinity when the other does, we see that the $R_\lambda \to \infty$ limit preserves the asymptotic constancy even if it yields a different limit from (3.12). The limit in this case is

$$\lim_{R_\lambda\to\infty} \frac{\langle\phi^2\rangle}{\langle\chi\rangle T'} = \tfrac{3}{2}c_1 \equiv \tfrac{3}{2}C_{OC} \qquad (0 < Sc < \infty). \tag{3.19}$$

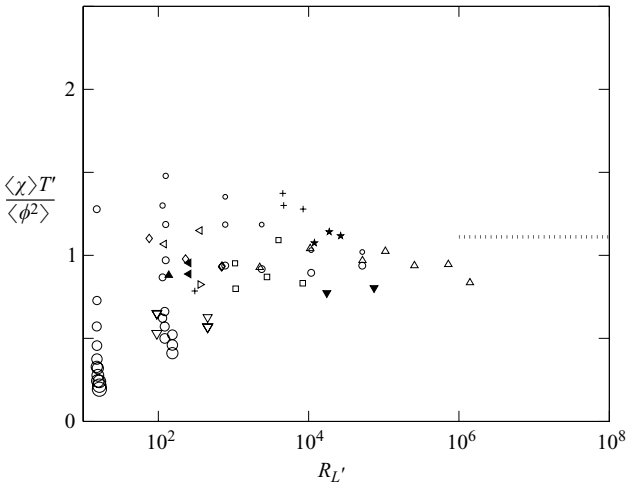

FIGURE 10. Scalar dissipation rate normalized by $T' = L^{2/3}/\langle\varepsilon\rangle^{1/3}$. Symbols as in figure 3. The relative size of the symbol illustrate the relative magnitude of Sc. Dotted line: the limit $2/3C_{OC}$ predicted by (3.19) with $C_{OC} = 0.6$.

In particular, the constant $3C_{OC}/2$ is independent of the flow details for high R_λ flows, and hence universal. The replot of the data using this scaling, shown in figure 10, seems to confirm the conclusion. The lack of strict universality could be due, among other effects, to the remnant effects of the large-scale details – especially considering the number of flows analysed here.

3.4. *The overall picture*

Equations (3.8) and (3.10) can be used to address the following question: how close is a given flow, characterized by given values of R_λ and Sc, to being asymptotic? To illustrate this point, we take the operational view that the asymptotic state is attained when the second term in each of these equations, which depends on both viscosity and diffusivity, is 10 % of the respective first terms. A choice of some other similar percentage will not affect the conclusions qualitatively, as we shall see.

In figure 11, we have plotted in the (R_λ, Sc)-plane the condition just spelled out, implementing it as follows. The full curve to the right-hand side of the plot is the locus of points for which the first term in (3.8) is 10 times larger than the log-term, while that to the left is the locus for which the first term of (3.10) is 10 times the second one. The dash-dotted lines mean that the R_λ-parts in the first term (which are small for large R_λ in any case) are neglected. The horizontal dotted line represents the R_λ at which the asymptotic state for $\langle\varepsilon\rangle$ has been attained (at this R_λ, the difference between (1.1) and its asymptotic value is $\frac{1}{10}$th of the latter). The behaviours bound the asymptotic state and, as long as a point resides above these lines, it can be regarded, to this rough approximation, as belonging to the asymptotic state. The diagram reinforces the statement that such an asymptotic state is governed by both Reynolds and Schmidt numbers, and that the precise criteria depend on whether Sc is large or small. The high-R_λ approximations (dash-dotted lines in the diagram) are very close to the solid lines. The approximation depends only on the flow-specific constant A (see (1.1)). However, since the constant A does not depend too strongly on the flow, these limits provide a qualitative indication for all flows. Moreover, if this

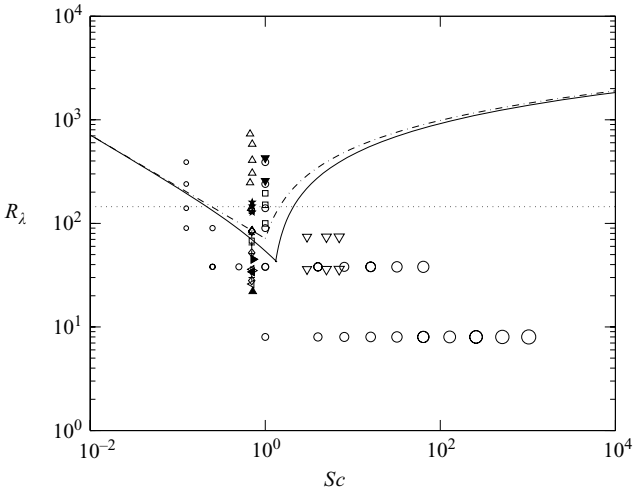

FIGURE 11. Theoretical limits for asymptotic state. See text for explanation on different lines. Symbols as in figure 3.

diagram were redrawn using $R_{L'}$ instead of R_λ (to make the result flow-independent), the result would look very similar.

Figure 11 also shows where all the data from our tables lie on this phase plane. It is clear that all the high-Sc data from simulations are not asymptotic, as also some of the older experiments. This is not a new revelation, but the diagram is the first attempt made to quantify this feature.

3.5. *A useful correlation*

We may write from dimensional considerations that

$$E_\theta(k) = C\langle\chi\rangle\langle\varepsilon\rangle^{-1/3}k^{-5/3}f(k\eta, Sc), \tag{3.20}$$

and

$$E_\theta(k) = C\langle\chi\rangle(\nu/\langle\varepsilon\rangle)^{1/2}k^{-1}f(k\eta, Sc), \tag{3.21}$$

depending on whether $Sc < 1$ or $Sc > 1$. We can then integrate these expressions to obtain $\langle\phi^2\rangle$

$$\frac{\langle\phi^2\rangle/\langle\chi\rangle}{\tau_\phi} = \int_0^\infty f(k\eta, Sc)\,\mathrm{d}(k\eta_B), \tag{3.22}$$

where τ_ϕ is equal to $\tau_\eta = (\nu/\langle\varepsilon\rangle)^{1/2}$ or $\tau_B = \langle\varepsilon\rangle^{-1/3}{\eta_B}^{2/3}$ depending on whether we use (3.20) or (3.21). Following the arguments leading to (3.10), we may expect that the right-hand side of (3.22) is a function of R_λ and Sc. Or, using $R_{L'}$ instead of R_λ, we have

$$\frac{\langle\phi^2\rangle/\langle\chi\rangle}{\tau_\phi} = F(R_{L'}, Sc). \tag{3.23}$$

We may now naively expect that F will be in the form of power laws in $R_{L'}$ and Sc and write

$$\frac{\langle\phi^2\rangle/\langle\chi\rangle}{\tau_\phi} = \alpha {R_{L'}}^n Sc^m. \tag{3.24}$$

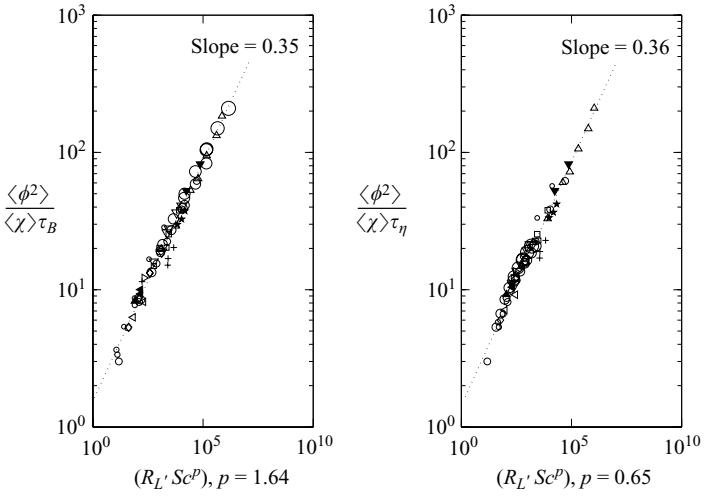

FIGURE 12. Scalar dissipation rate normalized with τ_B and τ_η for all data. Dotted lines are best fits. Symbols as in figure 3. The relative size of the symbols illustrate the relative magnitude of Sc.

By an optimization procedure, we obtain $n = 0.35$ and $m = 0.57$ (when using τ_B) and $n = 0.36$ and $m = 0.23$ (when using τ_η) as best fits to the data. This is confirmed in figure 12. The prefactor α in (3.24) is 1.55 for τ_B and 1.43 for τ_η (and the additive constants in both cases are negligibly small).

Using the fact that $\tau_B = (\nu/\langle\varepsilon\rangle)^{1/2} Sc^{-1/3} = T'/(15\ R_{L'}{}^2 Sc^2)^{1/6}$, (3.24) can also be written as

$$\frac{\langle\phi^2\rangle}{\langle\chi\rangle T'} \sim R_{L'}{}^{n-1/3} Sc^{m-1/3}. \tag{3.25}$$

The closeness of the best estimate of $1/3$ for n suggests that the R_λ-variation must indeed be negligible. The weak power of Sc is qualitatively similar to a logarithmic dependence on Sc as $Sc \to \infty$.

4. Summary of conclusions

We are concerned here with the asymptotic independence of the scalar dissipation on scalar diffusivity. One of the problems faced while attempting to understand the large-Reynolds number behaviour for non-unity Schmidt numbers is the lack of a suitable criterion of what constitutes the asymptotic state. Without that rough guideline, we can come to varying conclusions from simulations and experiments. In this paper we have arrived at empirical criteria based on the analysis of existing data and summarized them in figure 11.

We wish to note that the flows analysed here are homogeneous. This choice was deliberate because the situation with inhomogeneous flows is more complex. At the least, the meaning of when a Reynolds number is high enough depends on the flow. The presence of solid boundaries introduces additional complexities: the role of viscosity in the boundary layer is different from that in the jet (or wake) because the viscosity effects in the former will not vanish at any Reynolds number (though Schmidt number effects may vanish at high enough Sc). Our expectation is that the asymptotic independence discussed here will hold for all flows far from a solid boundary, but

that the rate at which this state is attained will be different for different flows. As we have already noted, the asymptotic value of the normalized scalar dissipation will depend on the flow. The exercise of examining inhomogeneous flows for the energy dissipation has been undertaken by Sreenivasan (1995), and is worth pursuing for the scalar as well. This has been an ongoing project of ours.

We acknowledge support from the National Science Foundation, via Grants CTS-0121030 (PKY) and CTS-0121007 (KRS), as well as via NSF cooperative agreement ACI-9619020 through computing resources provided by the National Partnership for Advanced Computational Infrastructure at the San Diego Supercomputer Center. We thank T. Gotoh for providing an early copy of Watanabe & Gotoh (2004), D. Bogucki for providing detailed numbers in relation to Bogucki *et al.* (1997), and R. W. Bilger, J. G. Brasseur and B. L. Sawford for helpful comments.

REFERENCES

Antonia, R. A., Zhou, T. & Xu, G. 2000 Second-order temperature and velocity structure functions: Reynolds number dependence. *Phys. Fluids* **12**, 1509–1517.

Batchelor, G. K. 1953 *The Theory of Homogeneous Turbulence*, Cambridge University Press.

Batchelor, G. K. 1959 Small-scale variation of convected quantities like temperature in turbulent fluid. *J. Fluid Mech.* **5**, 113–133.

Bilger, R. W. 2004 Some aspects of scalar dissipation. *Turb. Flow Combust.* **72**, 93–114.

Bogucki, D., Domaradzki, J. A. & Yeung, P. K. 1997 Direct numerical simulations of passive scalars with $Pr > 1$ advected by turbulent flow. *J. Fluid Mech.* **343**, 111–130.

Borgas, M. S., Sawford, B. L., Xu, S., Donzis, D. A. & Yeung, P. K. 2004 High Schmidt number scalars in turbulence: structure functions and Lagrangian theory. *Phys. Fluids* **16**, 3888–3899.

Brethouwer, G., Hunt, J. C. R. & Nieuwstadt, F. T. M. 2003 Micro structure and Lagrangian statistics of the scalar field with a mean gradient in isotropic turbulence. *J. Fluid Mech.* **474**, 193–225.

Constantin, P. 1994 Geometric statistics in turbulence. *SIAM Rev.* **36**, 73–98.

Corrsin, S. 1951 On the spectrum of isotropic temperature fluctuations in an isotropic turbulence. *J. Appl. Phys.* **22**, 469–473.

Doering, C. R. & Foias, C. 2002 Energy dissipation in body-forced turbulence. *J. Fluid Mech.* **467**, 289–306.

Eswaran, V. & Pope, S. B. 1988 An examination of forcing in direct numerical simulations of turbulence. *Comput. fluids* **16**, 257–278.

Fox, R. O. 2003 *Computational Models for Turbulent Reacting Flows.* Cambridge University Press.

Kaneda, Y., Ishihara, T., Itakura, K. & Uno, A. 2003 Energy dissipation rate and energy spectrum in high resolution direct numerical simulations of turbulence in a periodic box. *Phys. Fluids* **15**, L21–L24.

Kolmogorov, A. N. 1941 The local structure of turbulence in an incompressible viscous fluid for very large Reynolds numbers. *Dokl. Akad. Nauk. SSSR* **32**, 16–18. Reproduced in *Proc. R. Soc. Lond.* A **434**, 15–17.

Mills, R. R., Kistler, A. L., O'Brien, V. & Corrsin, S. 1958 Turbulence and temperature fluctuations behind a heated grid. *NACA TN* 4288.

Monin, A. S. & Yaglom, A. M. 1975 *Statistical Fluid Mechanics*, vol. 2. MIT Press.

Mydlarski, L. & Warhaft, Z. 1998 Passive scalar statistics in high-Péclet-number grid turbulence. *J. Fluid Mech.* **358**, 135–175.

Obukhov, A. M. 1949 The structure of the temperature field in a turbulent flow. *Izv, Nauk. SSSR. Geophys.* **13**, 58–69.

Overholt, M. R. & Pope, S. B. 1996 Direct numerical simulation of a passive scalar with imposed mean gradient in isotropic turbulence. *Phys. Fluids* **8**, 3128–3148.

Pumir, A. 1994 A numerical study of the mixing of a passive scalar in three dimensions in the presence of a mean gradient. *Phys. Fluids* **6**, 2118–2132.

Rogallo, R. S. 1981 Numerical experiments in homogeneous turbulence. *NASA TM* 81315.

Schumacher, J., Sreenivasan, K. R. & Yeung, P. K. 2003 Schmidt number dependence of derivative moments for quasi-static straining motion. *J. Fluid Mech.* **479**, 221–230.

Sirivat, A. & Warhaft, Z. 1983 The effect of a passive cross-stream temperature gradient on the evolution of temperature variance and heat flux in grid turbulence. *J. Fluid Mech.* **128**, 323–346.

Sreenivasan, K. R. 1984 On the scaling of the turbulence energy dissipation rate. *Phys. Fluids* **27**, 1048–1051.

Sreenivasan, K. R. 1995 The energy dissipation rate in turbulent shear flows. In *Developments in Fluid Mechanics and Aerospace Sciences* (ed. S. M. Deshpande, A. Prabhu, K. R. Sreenivasan & P. R. Viswanath), pp. 159–190. Interline.

Sreenivasan, K. R. 1998 An update on the dissipation rate in homogeneous turbulence. *Phys. Fluids* **10**, 528–529.

Sreenivasan, K. R. 2004 Possible effects of small-scale intermittency in turbulent reacting flows. *Flow Turb. Combust.* **72**, 115–131.

Sreenivasan, K. R., Antonia, R. A. & Danh, H. Q. 1977 Temperature dissipation fluctuations in a turbulent boundary layer. *Phys. Fluids* **20**, 1238–1249.

Sreenivasan, K. R., Tavoularis, S., Henry, R. & Corrsin, S. 1980 Temperature fluctuations and scales in grid-generated turbulence. *J. Fluid Mech.* **100**, 597–621.

Sreenivasan, K. R. & Yeung, P. K. 2000 Dissipation anomaly in passive scalars. *Bull. Am. Phys. Soc.* **45**, 107.

Tavoularis, S. & Corrsin, S. 1981 Experiments in nearly homogeneous shear flow with a uniform mean temperature gradient. Part 1. *J. Fluid Mech.* **104**, 311–347.

Taylor, G. I. 1938 Production and dissipation of vorticity in a turbulent fluid. *Proc. R. Soc. Lond.* A **164**, No. 918, 15–23.

Villermaux, E., Innocenti, C. & Duplat, J. 2001 Short circuits in the Corrsin–Obukhov cascade. *Phys. Fluids* **13**, 284–289.

Wang, L. P., Chen, S. & Brasseur, J. G. 1999 Examination of hypotheses in the Kolmogorov refined turbulence theory through high-resolution simulations. Part 2. Passive scalar field. *J. Fluid Mech.* **400**, 163–197.

Warhaft, Z. & Lumley, J. L. 1978 An experimental study of the decay of temperature fluctuations in grid-generated turbulence. *J. Fluid Mech.* **88**, 659–684.

Watanabe, T. & Gotoh, T. 2004 Statistics of passive scalar in homogeneous turbulence. *New J. Phys.* **6**, Art. 40.

Xu, G., Antonia, R. A. & Rajagopalan, S. 2000 Scaling of mean temperature dissipation rate. *Phys. Fluids* **12**, 3090–3093.

Yeh, T. T. & Van Atta, C. W. 1973 Spectral transfer of scalar and velocity fields in heated-grid turbulence. *J. Fluid Mech.* **58**, 233–261.

Yeung, P. K. & Pope, S. B. 1989 Lagrangian statistics from direct numerical simulations of isotropic turbulence. *J. Fluid Mech.* **207**, 531–586.

Yeung, P. K. & Sawford, B. L. 2002 Random sweeping hypothesis for passive scalars in isotropic turbulence. *J. Fluid Mech.* **459**, 129–138.

Yeung, P. K. & Zhou, Y. 1997 Universality of the Kolmogorov constant in numerical simulations of turbulence. *Phys. Rev.* E **56**, 1746–1752.

Yeung, P. K., Xu, S. & Sreenivasan, K. R. 2002 Schmidt number effects on turbulent transport with uniform mean scalar gradient. *Phys. Fluids* **14**, 4178–4191.

Yeung, P. K., Xu, S., Donzis, D. A. & Sreenivasan, K. R. 2004 Simulations of three-dimensional turbulent mixing for Schmidt numbers of the order 1000. *Flow Turb. Combust.* **72**, 333–347.

Zocchi, G., Tabeling, P., Maurer, J. & Willaime, H. 1994 Measurement of the scaling of the dissipation at high Reynolds numbers. *Phys. Rev.* E **50**, 3693–3700.